Elemental Sulfur as a Cathode Additive for Enhanced Rate Capability of Layered Lithium Transition Metal Oxides

Sheng S. Zhang,[1,z] Ji Chen,[2] and Chunsheng Wang[2,*]

[1] *Electrochemistry Branch, RDRL-SED-C, Sensors and Electron Devices Directorate, U.S. Army Research Laboratory, Adelphi, Maryland 20783-1138, USA*
[2] *Department of Chemical and Biomolecular Engineering, University of Maryland, College Park, Maryland 20742, USA*

Layered lithium transition metal oxides face two intrinsic problems of (1) oxygen evolution at high potentials or high temperatures and (2) the presence of alkaline Li residual compounds, to which nearly all known concerns with this class of cathode materials can be attributed. By selecting $LiNi_{0.80}Co_{0.10}Mn_{0.10}O_2$ (NCM811) as an example, here we dissolve small amount of elemental sulfur into the cathode slurry, finding that sulfur provides two beneficial functions in improving the electrochemical performance of NCM811 cathode. In the slurry-making process, sulfur reduces Ni^{3+} ions to produce a protective NiO layer and $Li_2S_2O_3$. In the initial charging process, the resultant $Li_2S_2O_3$ is electrochemically oxidized to Li_2SO_4, and meanwhile the Li residual compounds on the particle surface are removed. It is found that adding 0.25∼0.50 wt% (vs. NCM811) sulfur into the cathode slurry significantly enhances rate capability of Li/NCM811 cells although improvement on capacity retention is not visible. Impedance analysis explains that the enhanced rate capability is attributed to considerable reduction in both of the surface layer resistance and charge-transfer resistance. The results of this work indicate that sulfur additive provides a simple and practically feasible strategy for improving performances of the layered cathode materials.

 [DOI: 10.1149/2.0101904jes]

Manuscript submitted December 18, 2018; revised manuscript received January 29, 2019. Published February 9, 2019.

Layered lithium transition metal oxides have been intensively studied as the cathode material of high energy density Li-ion batteries due to their high capacity and low cost.[1–3] However, this class of cathode materials suffer two intrinsic problems of (1) oxygen evolution at high potentials or high temperatures and (2) inevitable presence of strongly alkaline Li residual compounds, mainly Li_2O, LiOH, and Li_2CO_3.[4] Nearly all performance degradations of the Li-ion batteries with layered cathode materials can be ultimately attributed to the above two intrinsic problems, such as irreversible phase transition from hexagonal through cubic to rocksalt structure,[5–7] mechanical crack of the secondary particle structure,[8–10] electrolyte depletion that is often accompanied by impedance increase and volumetric swelling of the batteries,[11,12] as well as gelation of cathode slurry in the slurry-making process.[13,14] For the Ni-rich layered cathode materials, a number of strategies have been explored to overcome the issues in relation to the oxygen evolution, such as cation doping for stabilizing the material's lattice structure,[15–17] surface coating for protecting cathode particles from parasitic reactions with the electrolyte components,[18–24] synthesizing concentration-gradient[25] or core-shell[26,27] materials with high Ni content core for stabilizing the material's surface chemistry, as well as using electrolyte[28] or cathode[29] additives for chemically trapping the released oxygen. Of particular interest, Yang et al.[30] reported that pre-cycling Li/$LiNi_{0.80}Co_{0.10}Mn_{0.10}O_2$ (NCM811) cells to 4.5 V for several cycles can in-situ produce a nano-thickness cubic phase NiO layer on the surface of NCM811 particles, which consequently protects electrolyte solvents from oxidative decomposition and hence extends the cells' cycle life. This can be considered to be the simplest and most practically viable strategy, reported up to date, for improving performances of the NCM811 cathode materials.

With respect to the surface Li residual compounds, a simple washing process in water followed by a heating treatment has shown to be very effective in removing the water-soluble Li residues.[31,32] Alternatively, the strongly akaline Li residual compounds can be converted to moderately alkaline Li_3PO_4 by treating the layered cathode materials with controlled amount of acidic H_3PO_4[33] or $(NH_4)_2HPO_4$[18,34] in an alcohol solution. In most cases, surface coating[19,24,35] and removing the surface Li residual compounds[18,31–34] are shown not only to stabilize capacity retention but also to enhance rate capability of the layered cathode materials. Without exceptions, however, all the above strategies require additional precipitating (or washing) and heating processes, which adds extra cost for the battery manufacture.

Without affecting the anode, electrolyte, and the procedure of battery manufacture, cathode additive is considered to be a more practically feasible means for improving performances of the layered cathode materials. In this effort,[36] we recently dissolved small amount of $LiPF_6$ into cathode slurry in the coating process, finding that the $LiPF_6$ additive readily reacts with surface Li residual compounds to form a LiF-rich LiF-Li_3PO_4 surface layer, which consequently improves cycling stability and rate capability of the Li/NCM811 cells. Inspired by this success, we here propose dissolving small amount of elemental sulfur into the cathode slurry by assuming that sulfur is able to provide the following two functions in affecting the performances of NCM811 cathode. In the coating process sulfur reduces Ni^{3+} ions on the NCM811 particle surface to form a NiO/$Li_2S_2O_3$ surface layer, and in the initial charging process the resultant $Li_2S_2O_3$ is electrochemically oxidized to stable Li_2SO_4, and meanwhile strongly alkaline Li_2O and Li_2CO_3 residues are removed from the cathode particle surface. By adding 0.25∼0.50 wt% (vs. the mass of NCM811) sulfur into the cathode slurry, we found that the rate capability of Li/NCM811 cells was significantly improved although improvement on the capacity retention is not visible. In this paper, we demonstrate the effect of elemental sulfur on the electrochemical property of NCM811 cathode material, and discuss the mechanism of sulfur additive in affecting performance of the NCM811 cathode material.

Experimental

NCM811 powder was purchased from MTI Corporation (Richmond, CA) and baked at 150°C in a vacuum oven for 2 h. A solution of 1.0 mol kg^{-1} $LiPF_6$ dissolved in a 3:7 (wt) blend of ethylene carbonate and ethyl methyl carbonate was used as the electrolyte. For sulfur treatment, a 0.50 wt% sulfur solution in N-methyl pyrrolidinone (NMP) was prepared as the sulfur source, and pure NMP was used as the additional solvent. Using calculated amounts of 0.50% sulfur solution and NMP solvent, a 0.50% S-treated NCM811 sample was prepared for structural characterizations by violently shaking an NCM811-S-NMP suspension on a 5100 Mixer Mill (SPEX CertiPrep) for 75 min, followed by filtering and drying the solid at 120°C under vacuum for 10 h. For comparison, the pristine sample was prepared using the same procedure without sulfur. X-ray powder diffraction (XRD) patterns of the samples were acquired by a D8 advance X-ray diffractometer (Bruker, USA). Morphology and elemental maps of

*Electrochemical Society Member.
[z]E-mail: shengshui.zhang.civ@mail.mil; shengshui@gmail.com

the samples were observed and acquired by an SU-70 field-emission scanning electron microscope (SEM, Hitachi, Japan). X-ray photoelectron spectroscopy (XPS) data of the samples were collected and analyzed by an AXIS 165 spectrometer (Kratos Analytical Ltd, UK) with the binding energy calibrated to 284.8 eV of the C 1s peak.

By adjusting the amounts of 0.50% sulfur solution and NMP solvent, the cathodes without and with sulfur were coated onto an aluminum foil in the composition of 80% NCM811, 10% Super-P carbon, and 10% PVDF. Resultant cathode sheets were punched into circular disks with a 1.27 cm^2 area, and dried at 120°C under vacuum for 10 h. On average, the loading of NCM811 was 8.2∼8.5 mg cm^{-2}. Using Celgard 2400 membrane as the separator, Li/NCM811 coin cells were assembled and cycled on a Maccor Series 4000 tester. In all cells a fixed 40 μL electrolyte was filled, and before testing the cells were formed at 0.1C between 3.0 V and 4.5 V for two cycles. The cells were cycled at 0.5C by charging to a pre-set cutoff voltage and then holding at the cutoff voltage until the current declined to 0.1C. To determine rate capability, the cells were discharged either galvanostatically at specific rates to 2.8 V or potentostatically at a specific voltage for 1 h. The 1 C-rate was referenced to a current of 200 mA g^{-1} NCM811.

AC-impedance of the Li/NCM811 cells was measured at 20°C using a Solartron SI 1287 Electrochemical Interface combined with a Solartron SI 1260 Impedance/Gain-Phase Analyzer. Stable measuring point was obtained by charging the cell at 0.1C to 4.3 V for the charged state and discharging the cell at 0.1C to 3.0 V for the discharged state, followed by a 1 h rest at open-circuit voltage (OCV). The impedance was measured at OCV with a 10 mV perturbation in frequency range from 100,000 Hz to 0.01 Hz. The acquired impedance spectra were analyzed using a CorrView software.

Results and Discussion

Role of sulfur additive in Li-ion battery.—Ni, Co, Mn in NCM811 are present in forms of Ni^{3+}/Ni^{2+}, Co^{3+}, and Mn^{4+} ions.[1–3] When coming into contact with the sulfur dissolved in cathode slurry, NCM811 can easily oxidize the dissolved sulfur to insoluble $Li_2S_2O_3$, while the transition metal ions are reduced to rocksalt phase MO (M = Ni, Co, or Mn) through a "solid-solution" two-phase reaction (Eq. 1), as evidenced by the XPS results (to be discussed later).

$$4LiMO_2 + 2S \rightarrow 4MO + Li_2S_2O_3 + Li_2O \quad [1]$$

In the same manner as reported by Yang et al.,[30] the resulting rocksalt phase MO can serve as a barrier to protect inner NMC811 from parasitic reactions with the electrolyte solvents. In the initial charging process (often called as "formation" in the Li-ion battery community), the $Li_2S_2O_3$ formed in Eq. 1 can be electrochemically oxidized to Li_2SO_4, and meanwhile the surface Li_2O and Li_2CO_3 residual compounds are removed as indicated by Eq. 2 and Eq. 3, respectively, leading to overall reactions of Eq. 4 and Eq. 5. The resultant CO_2 can be released together with other gases formed in the formation process of Li-ion batteries.

$$Li_2S_2O_3 + 5Li_2O - 8e \rightarrow 2Li_2SO_4 + 8Li^+ \quad [2]$$

$$Li_2S_2O_3 + 5Li_2CO_3 - 8e \rightarrow 2Li_2SO_4 + 5CO_2 + 8Li^+ \quad [3]$$

$$2LiMO_2 + S + 2Li_2O - 4e \rightarrow 2MO + Li_2SO_4 + 4Li^+ \quad [4]$$

$$2LiMO_2 + S + 2Li_2CO_3 - 4e \rightarrow 2MO + Li_2SO_4 + 2CO_2 + 4Li^+ \quad [5]$$

As indicated by the overall reactions of Eq. 4 and Eq. 5, sulfur additive on one hand reduces $LiMO_2$ to form a MO protective layer on the surface of NCM811 particles and on the other hand removes Li_2O and Li_2CO_3 residual compounds from the surface of NMC811 particles. The electrochemically stable Li_2SO_4 may be either coated onto the surface of NMC811 particles or presented as alone, and the extra Li^+ ions released by the sulfur treatment can be used to compensate for the loss of Li^+ ions as a result of the formation of solid electrolyte interphase in the graphite or silicon anode.

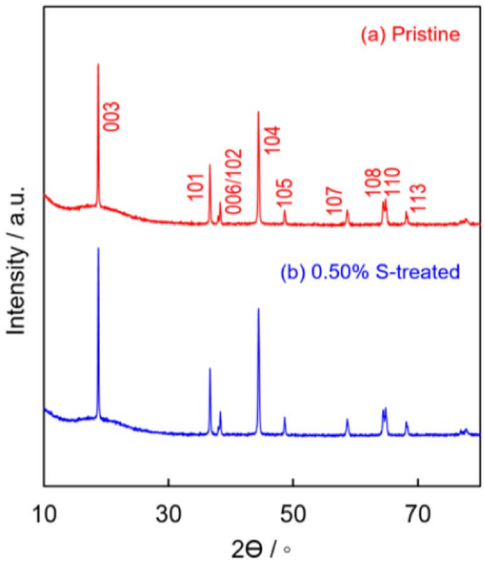

Figure 1. XRD patterns of NCM811 powder. (a) Pristine, and (b) 0.50% S-treated.

Structural characteristic of S-treated NCM811.—XRD patterns of the pristine and 0.5% S-treated samples are shown in Fig. 1, from which no difference can be observed except that both show characteristic diffraction peaks of the layered lithium transition metal oxides as indexed in the figure.[1–3] This means that sulfur treatment does not change crystalline structure of the NCM811 material, and that the amounts of MO, $Li_2S_2O_3$, and Li_2O produced by the sulfur treatment are too small to be detected by the XRD technique. Figs. 2a∼2d show SEM images of the pristine and 0.50% S-treated samples. In low magnification (Fig. 2a and Fig. 2c), there are no obvious differences in the morphology between two samples, both of which show a spherical agglomerate secondary structure that is assembled by numerous small primary particles. In high magnification (Fig. 2b and Fig. 2d), one sees that the surfaces of 0.50% S-treated sample are somewhat uneven, whereas those of the pristine sample are very smooth. As indicated by the small arrows in Fig. 2d, surfaces of the 0.50% S-treated NCM811 are partially etched, suggesting the reaction take place between sulfur and NCM811. In particular, Fig. 2e shows EDS mapping of a 0.50% S-treated NCM811 particle. It can be seen that the map of sulfur is well coincident with those of other elements and SEM. The above observations reveal that $Li_2S_2O_3$ formed by Eq. 1 is homogenously coated onto the surface of NMC811 particles, other than stayed alone in the intergranular spaces.

The surface chemistry of 0.50% S-treated NMC811 was characterized using XPS, and the S 2p and Ni $2p_{3/2}$ spectra are shown in Fig. 3. In the S 2p spectrum (Fig. 3a), there are three peaks of the binding energy at 162.7, 167.0, and 169.2 eV, respectively. With reference to the previous publications,[37,38] the peaks at 162.7 and 167.0 eV are assigned to two types of sulfur in $[S_2O_3]^{2-}$ ions, and the one at 169.2 eV to the sulfur in $[SO_4]^{2-}$ ions. According to the area of each peak, atomic percentages of these three types of sulfur are determined to be respectively 18.3%, 18.3%, and 63.4%. The Ni $2p_{3/2}$ spectrum (Fig. 3b) shows a main peak around 854.4 eV, which can be split into two peaks at 854.2 eV for Ni^{2+} ions and at 855.8 eV for Ni^{3+} ions, respectively.[30,39–43] According to the area of these two peaks, the atomic percentages of Ni^{2+} and Ni^{3+} ions are evaluated to be nearly equal (∼50%). Typically, the XPS probes ∼10 nm depth surfaces,[44] and atomic percentage of the Ni^{2+} ions in pristine NCM811 materials is in a 27∼28% range.[30,39] Much higher Ni^{2+} atomic percentage

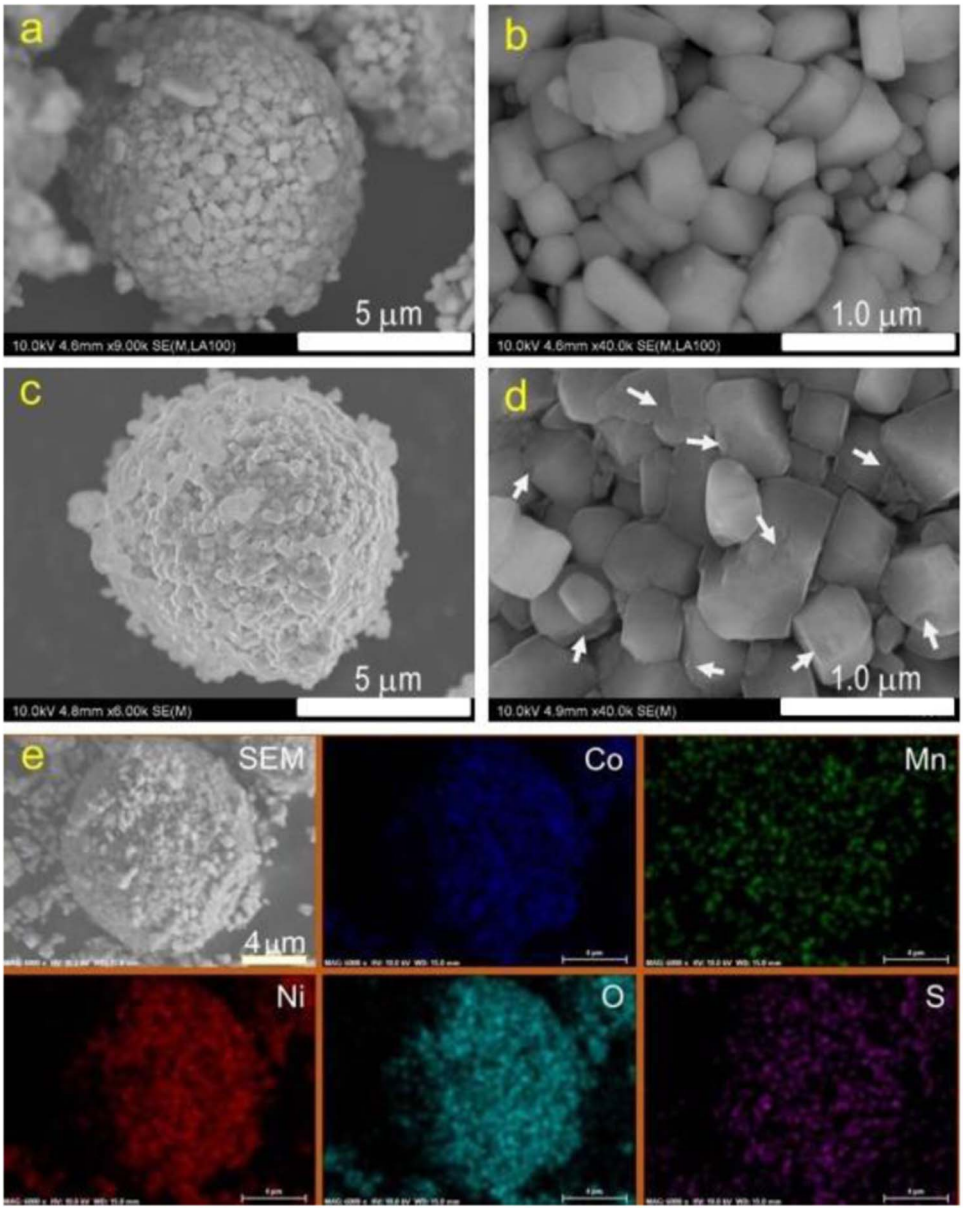

Figure 2. SEM images of NCM811 powder in different magnifications. (a and b) Pristine, (c and d) 0.50% S-treated, and (e) EDS mapping of 0.50% S-treated NCM811.

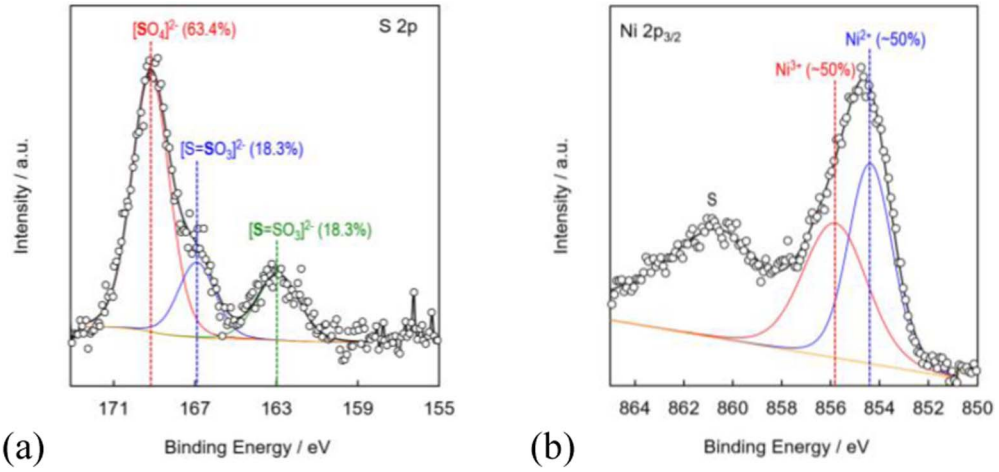

Figure 3. XPS spectra of 0.50% S-treated NCM811. (a) S 2p, and (b) Ni $2p_{3/2}$.

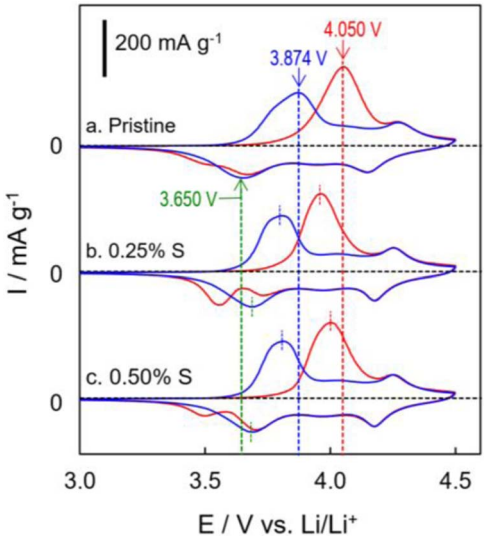

Figure 4. Cyclic voltammograms of the first two cycles for Li/NCM811 cells at 0.1 mV s^{-1} (1st cycle in red color and 2nd cycle in blue color). (a) Pristine, (b) 0.25% S-treated, and (c) 0.50% S-treated.

(~50%) detected in the 0.50% S-treated sample suggests that significant amount of Ni^{3+} ions on the NCM811 particle surface had been reduced to rocksalt phase NiO by the sulfur additive, as proposed by Eq. 1.

Electrochemical property.—Effect of sulfur additive on the electrochemical properties of NCM811 material was first evaluated using cyclic voltammetry, and results of the initial two cycles are displayed in Fig. 4. While the CV profiles are very similar, obvious differences in the redox potential can be found between the pristine and S-treated samples. In the first cycle (red color), oxidation current peak potentials for the hexagonal-monoclinic (H1-M) phase transition[45,46] are 4.05 V, 3.95 V, and 4.02 V for the pristine, 0.25% S-treated, and 0.50% S-treated sample, respectively. In the second cycle (blue color), these potentials are changed to 3.87, 3.78, and 3.79 V with the corresponding reduction current peak potentials equaling to 3.650, 3.672, and 3.701 V for the pristine, 0.25% S-treated, and 0.50% S-treated sample, respectively. The above results indicate that sulfur additive is able to reduce polarization of the charging and discharging processes of Li/NCM811 cells.

Cycling performance of the Li/NCM811 cells was evaluated by charging and discharging at 0.5C in two voltage ranges of 3.0–4.3 V and 3.0–4.5 V, respectively (Fig. 5). The sulfur additive appears not to improve capacity retention although it reduces polarization of the charging and discharging processes. In both cases, capacities of three cells with the pristine and S-treated NCM811 are fluctuated within the error ranges. When cycled in the 3.0–4.3 V range (Fig. 5a), three cells showed relatively stable capacities at ~160 mAh g^{-1}. When the voltage range was widened to 3.0–4.5 V (Fig. 5b), the initial capacity increased to 175~180 mAh g^{-1}, however, the capacity declined rapidly with cycle number. Acceleration in the capacity fading rate is mainly attributed to the oxygen evolution of delithiated NCM811 at high potentials, which triggers irreversible phase transition of the NCM811 material and chemical oxidation of the electrolyte solvents by the released oxygen. Since oxygen evolution at high potentials is an intrinsic nature of the layered cathode materials, it cannot be expected to be suppressed by the sulfur additive.

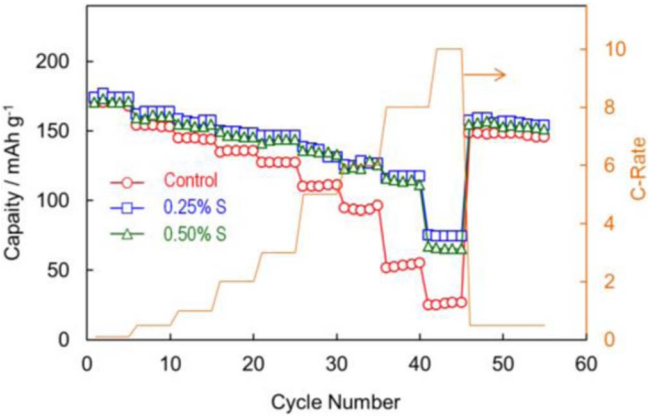

Figure 6. Rate capability of Li/NCM811 cells determined by charging at 0.5C to 4.3 V and discharging at specific rates to 2.8 V.

In line with the CV results, sulfur treatment shows significant improvement on the rate capability of Li/NCM811 cells as indicated in Fig. 6, which were determined by charging at 0.5C to 4.3 V and discharging at specific rates to 2.8 V. At low current rate (0.1C), three cells started with nearly same capacity (171–174 mAh g^{-1}). With an increase in the discharging current rate, however, the gap in capacities between the pristine and S-treated cells was gradually widened as a result of the IR polarization increasing with the current rate. For example, the capacities retained at 10C were respectively 17, 75, and 67 mAh g^{-1} for the pristine, 0.25% S-treated, and 0.50% S-treated cells. In another view, the rate capacity was examined by the potentostatic discharging technique, in which the cell was charged to 4.3 V and then discharged at a specific voltage for 1 h or until the current declined to 0.1C, whichever comes first. Fig. 7 compares the current-time responses of three cells recorded in potentostatically

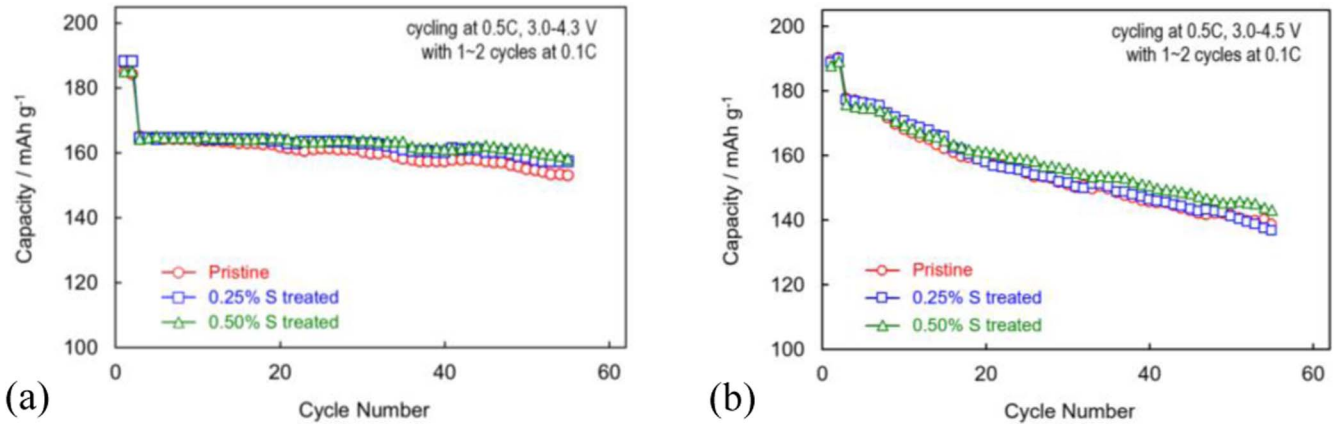

Figure 5. Cycling performance of Li/NCM811 cells at 0.5C in different voltage ranges. (a) 3.0–4.3 V, and (b) 3.0–4.5 V.

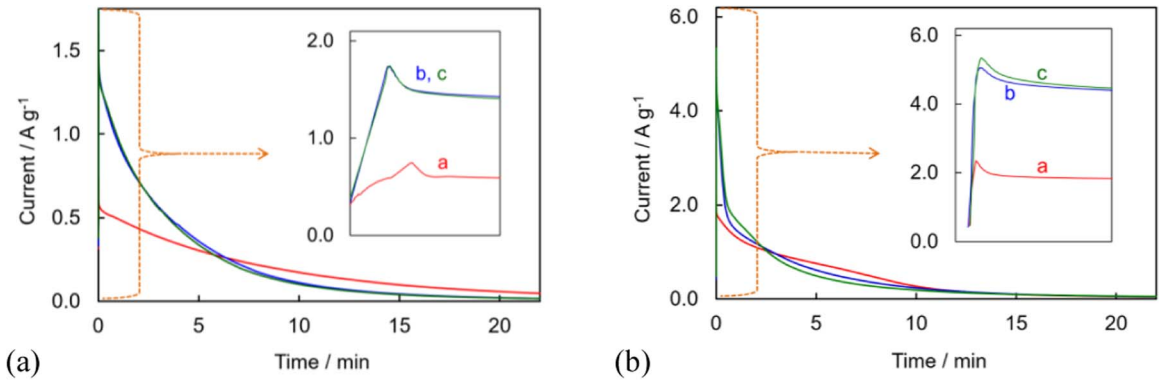

Figure 7. Rate capability of Li/NCM811 cells determined by potentostatic discharging at a specific voltage. (a) 3.8 V, and (b) 3.0 V. In each figure, (a) Pristine, (b) 0.25% S-treated, and (c) 0.50% S-treated.

discharging at 3.8 V and 3.0 V, respectively. Discharging at 3.8 V was set up to limit the capacity within the hexagonal-monoclinic (H3-H2-M) phase transitions region of NCM811,[45,46] whereas discharging at 3.0 V allows the cell to deliver full capacity. As observed from the inset of Fig. 7a and Fig. 7b, in both cases the 0.25% and 0.50% S-treated cells have almost same peak currents, and their peak currents are more than double of the pristine cell's peak current. By comparing the areas under the current-time curve of each cell in Fig. 7a, one sees that two S-treated cells have much higher capacity than the pristine cell, suggesting that the sulfur treatment is beneficial to the H3-H2-M phase transitions of NCM811 cathode material.

In order to understand the improvement of sulfur treatment on the rate capability, AC-impedance of the Li/NCM811 cells was analyzed. Typically, impedance of the Li metal cells is contributed by the bulk resistance (R_b), surface layer resistance (R_{sl}), and charge-transfer resistance (R_{ct}), and the R_{sl} and R_{ct} are reflected as two semicircles in the impedance spectrum.[47,48] Since the R_{sl} and R_{ct} change vastly with the cell's state-of-charge,[48] the impedance spectra at 4.3 V for the charged state and at 3.0 V for the discharged state were representatively measured and summarized in Fig. 8. In the charged state (Fig. 8a), the R_{sl} and R_{ct} in the S-treated cells are much smaller than those in the pristine cell. In the discharged state (Fig. 8b), the R_{ct} becomes indefinitely large so that its relative semicircle cannot be formed, however, much smaller R_{sl} still can be observed from the S-added cells, as compared with that of the pristine cell. The above results indicate that sulfur additive greatly reduces the surface layer resistance, which consequently increases the kinetics of electrode reaction, as suggested by the significantly reduced charge-transfer resistance.

Conclusions

Layered cathode materials face two intrinsic problems of (1) oxygen evolution at high potentials or high temperatures and (2) the presence of alkaline Li residual compounds on the particle surface. Aiming to mitigate the adverse effects caused by these two intrinsic problems, we proposed elemental sulfur as a cathode additive by selecting NCM811 as an example, and demonstrated two beneficial functions of sulfur additive in the Li-ion batteries. In the coating process, the dissolved sulfur reduces transition metal ions (M^{3+}) to rocksalt phase MO that serves as a surface barrier to prevent parasitic reactions between the cathode particles and electrolyte solvents. In the initial charging process, the resultant $Li_2S_2O_3$ is electrochemically oxidized to stable Li_2SO_4, and meanwhile the surface Li_2O and Li_2CO_3 residual compounds are removed with the resultant Li_2SO_4 being homogenously coated onto the cathode particle surface as an additional protective barrier. By dissolving 0.25% and 0.50%, respectively, of sulfur into the cathode slurry, we are able to observe that sulfur additive significantly enhances the rate capability of Li/NCM811 cells although improvement on the cycling stability is not visible. Impedance analysis reveals that the enhanced rate capability is attributed to considerable reduction in both of the surface layer resistance and charge-transfer resistance. The results of this work indicate that using sulfur

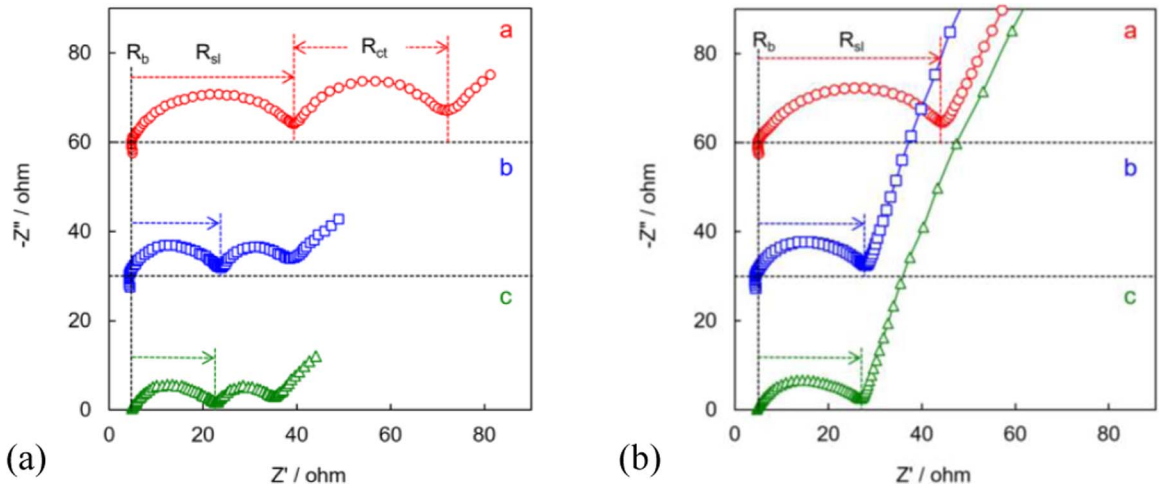

Figure 8. Impedance spectra of Li/NCM811 cells at charged state (a, 4.3 V) and discharged state (b, 3.0 V), respectively. In each figure, (a) Pristine, (b) 0.25% S-treated, and (c) 0.50% S-treated.

additive is a simple and practically feasible means for improving rate capability of the layered cathode materials.

Acknowledgments

The author (SZ) acknowledges support of the Army Research Laboratory, and thanks Dr. C. Lundgren for her critical reading of the manuscript and valuable comments.

ORCID

Sheng S. Zhang https://orcid.org/0000-0003-4435-4110

References

1. A. Manthiram, J. C. Knight, S. T. Myung, S. M. Oh, and Y. K. Sun, *Adv. Energy Mater.*, **6**(1), 1501010 (2016).
2. S. T. Myung, F. Maglia, K. J. Park, C. S. Yoon, P. Lamp, S. J. Kim, and Y. K. Sun, *ACS Energy Lett.*, **2**, 196 (2017).
3. J. Kim, H. Lee, H. Cha, M. Yoon, M. Park, and J. Cho, *Adv. Energy Mater.*, **8**, 1702028 (2018).
4. R. Jung, R. Morasch, P. Karayaylali, K. Phillips, F. Maglia, C. Stinner, Y. Shao-Horn, and H. A. Gasteiger, *J. Electrochem. Soc.*, **165**, A132 (2018).
5. S. M. Bak, E. Hu, Y. Zhou, X. Yu, S. D. Senanayake, S. J. Cho, K. B. Kim, K. Y. Chung, X. Q. Yang, and K. W. Nam, *ACS Appl. Mater. Interfaces*, **6**, 22594 (2014).
6. M. Dixit, B. Markovsky, F. Schipper, D. Aurbach, and D. T. Major, *J. Phys. Chem. C*, **121**, 22628 (2017).
7. H. H. Ryu, K. J. Park, C. S. Yoon, and Y. K. Sun, *Chem. Mater.*, **30**, 1155 (2018).
8. Y. Makimura, S. Zheng, Y. Ikuhara, and Y. Ukyo, *J. Electrochem. Soc.*, **159**, A1070 (2012).
9. S. Watanabe, M. Kinoshita, T. Hosokawa, K. Morigaki, and K. Nakura, *J. Power Sources*, **258**, 210 (2014).
10. H. Liu, M. Wolf, K. Karki, Y. S. Yu, E. A. Stach, J. Cabana, K. W. Chapman, and P. J. Chupas, *Nano Lett.*, **17**, 3452 (2017).
11. R. Jung, M. Metzger, F. Maglia, C. Stinner, and H. A. Gasteiger, *J. Electrochem. Soc.*, **164**, A1361 (2017).
12. R. Jung, M. Metzger, H. A. Gasteiger, R. Jung, F. Maglia, and C. Stinner, *J. Phys. Chem. Lett.*, **8**(19), 4820 (2017).
13. P. Kalyani and N. Kalaiselvi, *Sci. Technol. Adv. Mater.*, **6**, 689 (2005).
14. K. Park, J. H. Park, S. G. Hong, B. Choi, S. W. Seo, J. H. Park, and K. Min, *Phys. Chem. Chem. Phys.*, **18**, 29076 (2016).
15. B. Zhang, L. Li, and J. Zheng, *J. Alloys and Compd.*, **520**, 190 (2012).
16. U. H. Kim, E. J. Lee, C. S. Yoon, S. T. Myung, and Y. K. Sun, *Adv. Energy Mater.*, **6**, 1601417 (2016).
17. U. H. Kim, D. W. Jun, K. J. Park, Q. Zhang, P. Kaghazchi, D. Aurbach, D. T. Major, G. Goobes, M. Dixit, N. Leifer, C. M. Wang, P. Yan, D. Ahn, K. H. Kim, C. S. Yoon, and Y. K. Sun, *Energy Environ. Sci.*, **11**, 1271 (2018).
18. H. G. Song, J. Y. Kim, K. T. Kim, and Y. J. Park, *J. Power Sources*, **196**, 6847 (2011).
19. Y. Kim, *Phys. Chem. Chem. Phys.*, **15**, 6400 (2013).
20. P. Oh, B. Song, W. Li, and A. Manthiram, *J. Mater. Chem. A*, **4**, 5839 (2016).
21. J. Xie, A. D. Sendek, E. D. Cubuk, X. Zhang, Z. Lu, Y. Gong, T. Wu, F. Shi, W. Liu, E. J. Reed, and Y. Cui, *ACS Nano*, **11**, 7019 (2017).
22. L. Ma, Y. Li, Z. Chen, F. Zhang, P. Ding, L. Mao, and F. Lian, *ChemElectroChem*, **4**, 1443 (2017).
23. X. Ding, L. N. Xiao, Y. X. Li, Z. F. Tang, J. W. Wan, Z. Y. Wen, and C. H. Chen, *J. Power Sources*, **390**, 13 (2018).
24. F. Schipper, H. Bouzaglo, M. Dixit, E. M. Erickson, T. Weigel, M. Talianker, J. Grinblat, L. Burstein, M. Schmidt, J. Lampert, C. Erk, B. Markovsky, D. T. Major, and D. Aurbach, *Adv. Energy Mater.*, **8**, 1701682 (2018).
25. Y. K. Sun, S. T. Myung, B. C. Park, J. Prakash, I. Belharouak, and K. Amine, *Nat. Mater.*, **8**, 320 (2009).
26. Y. Cho, P. Oh, and J. Cho, *Nano Lett.*, **13**, 1145 (2013).
27. H. Kim, M. G. Kim, H. Y. Jeong, H. Nam, and J. Cho, *Nano Lett.*, **15**, 2111 (2015).
28. D. J. Lee, D. Im, Y. G. Ryu, S. Lee, J. Yoon, J. Lee, W. Choi, I. Jung, S. Lee, and S. G. Doo, *J. Power Sources*, **243**, 831 (2013).
29. S. S. Zhang and D. T. Tran, *J. Power Sources*, **403**, 167 (2018).
30. J. Yang and Y. Xia, *J. Electrochem. Soc.*, **163**, A2665 (2016).
31. J. Kim, Y. Hong, K. S. Ryu, M. G. Kim, and J. Cho, *Electrochem. Solid-State Lett.*, **9**, A19 (2006).
32. X. Xiong, Z. Wang, P. Yue, H. Guo, F. Wu, J. Wang, and X. Li, *J. Power Sources*, **222**, 318 (2013).
33. C. H. Jo, D. H. Cho, H. J. Noh, H. Yashiro, Y. K. Sun, and S. T. Myung, *Nano Research*, **8**, 1464 (2015).
34. X. Xiong, D. Ding, Y. Bu, Z. Wang, B. Huang, H. Guo, and X. Li, *J. Mater. Chem. A*, **2**(30), 11691 (2014).
35. X. Li, K. Zhang, M. Wang, Y. Liu, M. Qu, W. Zhao, and J. Zheng, *Sustainable Energy Fuels*, **2**, 413 (2018).
36. S. S. Zhang, X. Fan, and C. Wang, *ChemElectroChem*, under review, https://doi.org/10.1002/celc.201801858.
37. Q. Pang, D. Kundu, M. Cuisinier, and L. F. Nazar, *Nat. Commun.*, **5**, 4759 (2014).
38. X. Liang, C. Hart, Q. Pang, A. Garsuch, T. Weiss, and L. F. Nazar, *Nat. Commun.*, **6**, 5682 (2015).
39. F. Wu, J. Tian, Y. Su, J. Wang, C. Zhang, L. Bao, T. He, J. Li, and S. Chen, *ACS Appl. Mater. Interfaces*, **7**, 7702 (2015).
40. E. Zhao, M. Chen, Z. Hu, D. Chen, L. Yang, and X. Xiao, *J. Power Sources*, **343**, 345 (2017).
41. Q. Zhang, Y. Su, L. Chen, Y. Lu, L. Bao, T. He, J. Wang, R. Chen, J. Tan, and F. Wu, *J. Power Sources*, **396**, 734 (2018).
42. Y. Chen, Y. Li, W. Li, G. Cao, S. Tang, Q. Su, S. Deng, and J. Guo, *Electrochim. Acta*, **281**, 48 (2018).
43. Y. Su, Y. Yang, L. Chen, Y. Lu, L. Bao, G. Chen, Z. Yang, Q. Zhang, J. Wang, R. Chen, S. Chen, and F. Wu, *Electrochim. Acta*, **292**, 217 (2018).
44. B. Philippe, R. Dedryvere, J. Allouche, F. Lindgren, M. Gorgoi, H. Rensmo, D. Gonbeau, and K. Edstrom, *Chem. Mater.*, **24**, 1107 (2012).
45. W. Li, J. N. Reimers, and J. R. Dahn, *Solid State Ionics*, **67**, 123 (1993).
46. H. J. Noh, S. Youn, C. S. Yoon, Y. K. Sun, and J. Power Sources, **233**, 121 (2013).
47. S. S. Zhang, K. Xu, and T. R. Jow, *Electrochem. Solid-State Lett.*, **5**, A92 (2002).
48. S. S. Zhang, K. Xu, and T. R. Jow, *Electrochim. Acta*, **49**, 1057 (2004).